

H I in very metal-poor galaxies: the SBS 0335–052 system

B. Ekta,^{1*} Simon A. Pustilnik,^{2,3*} Jayaram N. Chengalur^{1*}

¹ National Centre for Radio Astrophysics, Post Bag 3, Ganeshkhind, Pune 411 007, India

² Special Astrophysical Observatory of RAS, Nizhnyj Arkhыз, Karachai-Circassia 369167, Russia

³ Isaac Newton Institute of Chile, SAO Branch, Nizhnyj Arkhыз, Russia

Accepted 2009 April 29. Received 2009 April 29; in original form 2009 March 4

ABSTRACT

We present Giant Metrewave Radio Telescope (GMRT), H I 21cm observations of SBS 0335–052E and SBS 0335–052W, a close pair of dwarf galaxies, which are further unusual in being the most metal-poor star-forming galaxies known. We present images at several angular resolutions, ranging from ~ 40 to 4 arcsec. These images show that SBS 0335–052 is a strongly interacting system, with a faint diffuse H I bridge seen at low resolution, and elongated tails seen at the higher resolutions. The overall morphology suggests that the pair represents a major (as both galaxies have similar H I masses) merger of extremely gas-rich galaxies, which is currently past the first close encounter. The low-resolution velocity field is dominated by the velocity difference between the two galaxies and the velocity gradient along the tidal features. However, for SBS 0335–052W at least, at high angular resolution, one sees a central velocity field that could be associated with the spin of the original undisturbed disc. The two galaxies have very similar H I masses, but very different optical properties and current star formation rates. A possible reason for this is the differing amounts of tidally-induced star formation, because of the different spin orientations of these interacting galaxies. The highest angular resolution H I images show that the ionized superbubble, identified by Thuan, Izotov & Lipovetsky (1997), in the Hubble Space Telescope (*HST*) images of SBS 0335–052E, is extended along one of the diffuse tidal features, and that there is a high-density H I clump at the other end of the superbubble. The star formation in SBS 0335–052E occurs mainly in a group of superstar clusters (SSCs) with a clear age gradient; the age decreases as one approaches the dense H I clump. We suggest that this propagating star formation is driven by the superbubble expanding into a medium with a tidally-produced density gradient. The high pressures associated with the compressed material would also naturally explain why current star formation is mainly concentrated in superstar clusters.

Key words: galaxies: dwarf – galaxies: evolution – galaxies: individual: SBS 0335–052 – galaxies: kinematics and dynamics – radio lines: galaxies

1 INTRODUCTION

Low-mass star-forming galaxies with metallicities of $Z_{\odot}/10$ and lower¹ (i.e., $12 + \log(\text{O}/\text{H}) \leq 7.65$; the so called ‘extremely Metal-Deficient’ (XMD) galaxies) are very rare in the local Universe (e.g., Kunth & Östlin 2000). According to Pustilnik et al. (2003), they comprise less than 2 per cent of all known emission-line galaxies. No more than half a dozen (of the tens of thousands of emission-line galaxies)

are known to have metallicities near the bottom of the metallicity-distribution ($Z \sim Z_{\odot}/35 - Z_{\odot}/25$). In this paper, we present GMRT H I observations of the SBS 0335–052 system, which contains the lowest known metallicity XMD galaxies. SBS 0335–052 consists of a galaxy pair, SBS 0335–052E and SBS 0335–052W, with a projected separation of ~ 22 kpc (Pustilnik et al. 2001). Both galaxies, in the pair, are extremely metal-poor, and have oxygen abundances, $12 + \log(\text{O}/\text{H}) \sim 7.29$ (SBS 0335–052E, Izotov et al. (1997) and references therein) and 7.12 (SBS 0335–052W, Izotov, Thuan & Guseva (2005) and references therein), respectively. The galaxies are also peculiar in that they have very blue colours in their outer parts (indicative of small ages even for the older stellar population, e.g.,

* ekta@ncra.tifr.res.in, sap@sao.ru, chengalu@ncra.tifr.res.in

¹ Throughout this paper, we use the new scale for solar metallicity, viz., Z_{\odot} corresponds to $12 + \log(\text{O}/\text{H}) = 8.66$ (Asplund et al. 2004).

Table 1. Parameters of the GMRT observations

Date of observations	2004 November 28, 29, December 10, 11, 12
Field center R.A.(2000)	03 ^h 37 ^m 44.0 ^s
Field center Dec.(2000)	−05° 02′ 40.0″
Central Velocity (km s ^{−1})	4040
Time on-source (h)	~20
Number of channels	128
Channel separation (km s ^{−1})	~3.3
Flux Calibrators	3C 48, 3C 147
Phase Calibrator	PKS J0323+0534
Resolution (arcsec ²) (root mean square (rms) noise in mJy Bm ^{−1})	43 × 39 (1.16)
	21 × 19 (0.85)
	9 × 9 (0.66)
	6 × 5 (0.55)
	3 × 3 (0.51)

Papaderos et al. (1998) and Pustilnik, Pramskij & Kniazev (2004)), and have the bulk of their baryonic material in the form of gas.

Observations of local, low-metallicity galaxies allow one to gain insight into the modes of star formation in primeval objects, where the physical conditions (e.g., low metallicity, large gas fraction, small gravitational potential, etc.) are likely to be similar. H I observations of local XMD galaxies have been presented by us (e.g., Nançay Radio Telescope data by Pustilnik & Martin (2007), and GMRT data by Chengalur et al. (2006) and Ekta, Chengalur, Pustilnik (2006)). In particular, Ekta, Chengalur, Pustilnik (2008) discuss the H I distribution, kinematics and star formation in three of the six most metal-poor star-forming galaxies, viz., DDO 68, UGC 772 (SDSS J0113+0052) and SDSS J2104–0035. In the case of SBS 0335–052, Very Large Array (VLA) H I 21cm observations have been presented earlier in Pustilnik et al. (2001). Our current GMRT observations are both deeper, and also cover a larger range of angular resolutions than the earlier VLA ones. Throughout this paper, we assume a distance of 53.6 Mpc for SBS 0335–052. At this distance, 1 arcsec corresponds to a linear distance of ~260 pc.

2 OBSERVATIONS AND DATA REDUCTION

SBS 0335–052 was observed in five different runs, on 2004 November 28, 29, December 10, 11, 12, at the GMRT, with a total bandwidth of 2 MHz, and a channel resolution of 15.6 kHz (which corresponds to a velocity resolution of ~3.3 km s^{−1}). The total on-source time was ~20 h. The flux calibrators, 3C 48 and 3C 147, and the phase calibrator, PKS J0323+0534 were observed at appropriate intervals. Each of the data sets was reduced in classic Astronomical Image Processing System (AIPS). The data reduction steps included flagging of the bad visibility points, calibrating for phase and bandpass shape. The visibility data from the different runs were combined into one data set using the task 'DBCON'. Since the differential Doppler shift between the different runs is small compared to the channel width, no Doppler correction was applied. After continuum subtraction, each channel was imaged using task 'IMAGR'. The parameters of the GMRT observations are given in Table 1.

3 H I MORPHOLOGY AND KINEMATICS

The integrated H I intensity map of SBS 0335–052 system, at an angular resolution of ~40 arcsec, is shown in Fig. 1(A). At this resolution, the two galaxies appear to be embedded in a common H I envelope. The earlier VLA observations (Pustilnik et al. 2001) also show the galaxies to be in a common envelope, but the total H I extent seen in our map (225 × 105 arcsec², or 58.5 × 27.3 kpc², at an H I column density level of 1.0 × 10¹⁹ atoms cm^{−2}) is smaller than that deduced from the VLA observations (65 × 22 kpc², after rescaling to the distance adopted here). Our H I maps are, at least, a factor of 1.5 times more sensitive than those from earlier VLA observations. The rms noise quoted by the latter is 1.0 mJy beam^{−1} per channel, for a channel width of 5.3 km s^{−1}, at an angular resolution of ~20 × 15 arcsec². Our maps, at slightly coarser resolution (~21 × 19 arcsec²), have an rms noise of 0.85 mJy beam^{−1} per channel, for a channel width of 3.3 km s^{−1}. The outermost contour, in Fig 1(A), is a factor of ~5 times lower than the sensitivity level in the VLA data. The difference in linear sizes seen at the GMRT and VLA is largely because a tentative feature (to the north-east of the main emission) seen in the VLA image has not been detected at the GMRT.

The GMRT H I velocity field, at ~40 arcsec, is shown in Fig. 1(B). There is an overall velocity gradient in northeast–southwest (NE–SW) direction. The contours are crowded in the region between the two galaxies. A contour map (at the same angular resolution) of every alternate channel, in the data cube, is shown in Fig. 2. H I emission, peaked at the location of each of the two galaxies, and an H I ‘bridge’, connecting the two galaxies (at intermediate velocities) can be seen.

Fig. 1 also shows the H I emission at two higher angular resolutions, viz., ~20 arcsec (panels C, D) and ~9 arcsec (panels E, F, G). In the ~20 arcsec image, the ‘bridge’ emission appears to be completely resolved out. To check if the ‘bridge’ emission seen in panel A is entirely due to beam smearing, we smoothed the ~20 arcsec map to 40 arcsec resolution, and compared it with the map shown in panel A. The smoothed map does not recover all the flux seen in the ‘bridge’ region in panel A, indicating that the emission seen is not entirely due to beam smearing. At ~20 arcsec resolution, one can clearly distinguish the H I associated with each galaxy. Both galaxies show extended elongated features, reminiscent of ‘tidal tails’. The velocity field of the SBS 0335–052 system, at a resolution of ~21 × 19 arcsec² in Fig. 1(D), shows complex patterns. Both galaxies have disturbed fields. In the case of SBS 0335–052E, there is a clear NE–SW velocity gradient, but the velocity contours show substantial deviations from those expected from a rotating disc. In the case of SBS 0335–052W, there is an overall NE–SW velocity gradient along the ‘tidal tails’, but in the central part of the galaxy, the velocity gradient is approximately from south to north.

At a still higher angular resolution (viz., ~9 arcsec, panel E), one can see more clearly that the gas distribution of each galaxy consists of a central peak coincident with the optical emission, along with elongated ‘tidal tail’ like features. In the case of SBS 0335–052W, one can also see that the central H I body is elongated in the north-north-west–south-south-east (NNW–SSE) direction (see also Fig. 5).

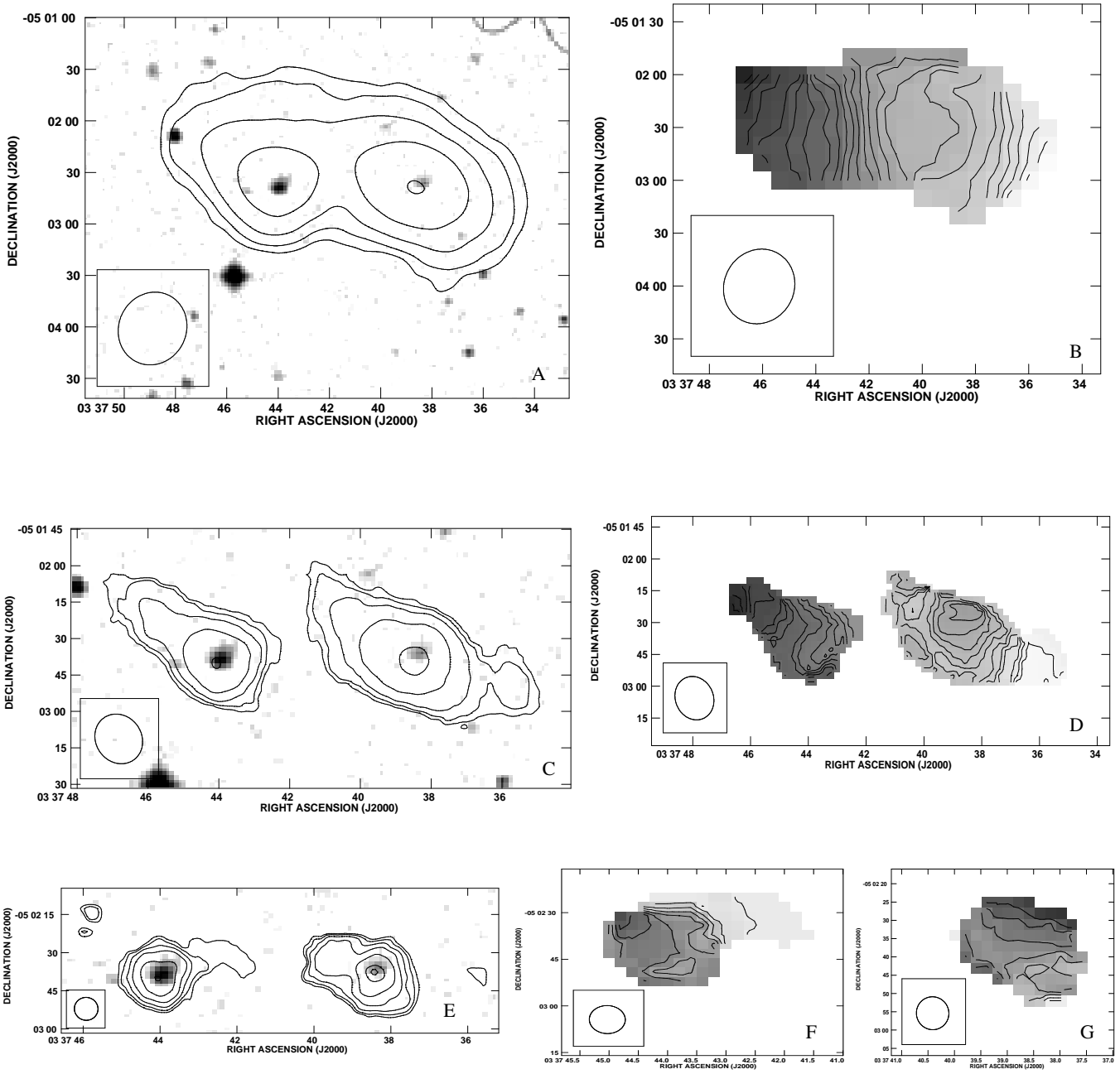


Figure 1. (A.) Integrated H I emission map of SBS 0335–052 system, in contours, at a resolution of $\sim 43 \times 39$ arcsec², overlaid on the *B*-band Digitized Sky Survey-II (DSS-II) image (grey-scale, arbitrary units). The contour levels are at H I column densities of $\sim 0.14, 0.31, 0.69, 1.52, 3.34 \times 10^{20}$ atoms cm⁻². (B.) The H I intensity-weighted velocity field (contours and grey-scales) at a resolution of $\sim 43 \times 39$ arcsec². The velocity contours are from 3997 to 4074 km s⁻¹, in steps of 3.3 km s⁻¹. (C.) Same as (A), excepting that the H I image is at an angular resolution of $\sim 21 \times 19$ arcsec². The contour levels are at H I column densities of 0.30, 0.67, 1.50, 3.33 and 7.40×10^{20} atoms cm⁻². (D.) Same as (B), excepting that the H I velocity field is at an angular resolution of $\sim 21 \times 19$ arcsec² resolution. The velocity contours range from 3997 to 4080 km s⁻¹, in steps of 3.3 km s⁻¹. (E.) Same as (A), excepting that the H I image is at an angular resolution of ~ 9 arcsec. The contour levels are at H I column densities of 0.75, 1.39, 2.57, 4.75, 8.78, 16.24 and 18.81×10^{20} atoms cm⁻². (F,G.) Same as (B), excepting that the H I velocity field is at an angular resolution of ~ 9 arcsec. In F, the velocity contours range from 4037 to 4060 km s⁻¹ (SBS 0335–052E), and in G, from 4013 to 4036 km s⁻¹ (SBS 0334–052W). The contour spacing is 3.3 km s⁻¹.

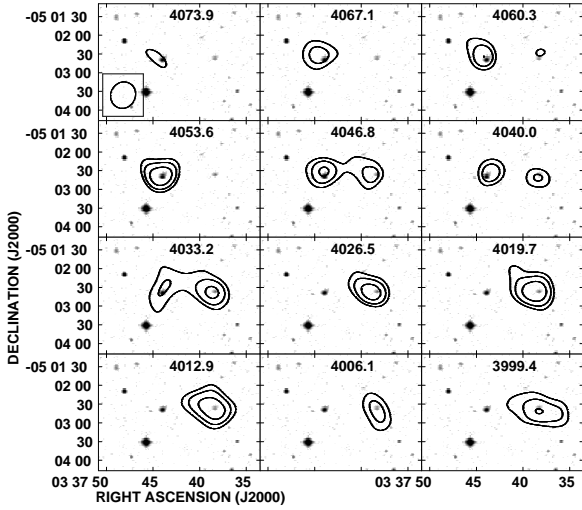


Figure 2. The channel maps of SBS 0335–052 system, in contours, at a resolution of $\sim 43 \times 39$ arcsec². The contours are at -3, 3, 4.2, 6.0 times the rms noise in a single channel (1.16 mJy beam⁻¹). Every alternate channel is shown. The *B*-band DSS-II image is shown in grey-scale, in arbitrary units. The velocity, for each shown channel, is given in corresponding panel.

The H I velocity field, at this resolution (panel G), shows that the velocity gradient in SBS 0335–052W is also approximately aligned with the major axis of the central H I distribution. This suggests that at this resolution one is beginning to see the gas associated with the disc of this galaxy. In the case of SBS 0335–052E, the dominant velocity gradient still seems to be along the tidal tail.

To summarize, our multi-resolution images show SBS 0335-052 to be strongly interacting, with a diffuse H I ‘bridge’ seen at low resolution, and elongated ‘tidal tails’ seen at the higher resolutions. The large-scale velocity field is largely dominated by the velocity of the tidal features, however, for SBS0335–052W at least, at the highest angular resolution, one sees a central velocity gradient that one could associate with the spin of the original undisturbed disc.

The spectra of SBS 0335–052E, SBS 0335–052W and the whole system (obtained from ~ 40 arcsec data) are shown in Fig. 3. The total integrated H I flux is 1.46 ± 0.15 Jy km s⁻¹, which matches, within error bars, with the value given in Thuan et al. (1999), viz., 1.28 ± 0.22 Jy km s⁻¹. The VLA observations (Pustilnik et al. 2001) obtained a higher value of 2.46 ± 0.18 Jy km s⁻¹. The reason for this discrepancy (which is at the $\sim 4\sigma$ level) is unclear. We have confirmed the amplitude calibration of the GMRT maps, by comparing the fluxes of background continuum sources in our map with their NRAO VLA Sky Survey (NVSS) fluxes. The H I fluxes measured for eastern and western components are 0.61 and 0.86 Jy km s⁻¹ (42 and 58 per cent of the total flux), respectively, corresponding to H I masses of 4.2 and $5.8 \times 10^8 M_{\odot}$, and an H I mass-ratio of 1:1.4. The central velocities of SBS 0335–052E and SBS 0335–052W are 4053.6 ± 1.7 , 4014.7 ± 1.7 km s⁻¹, respectively, and the velocity widths, at 50 per cent levels, are

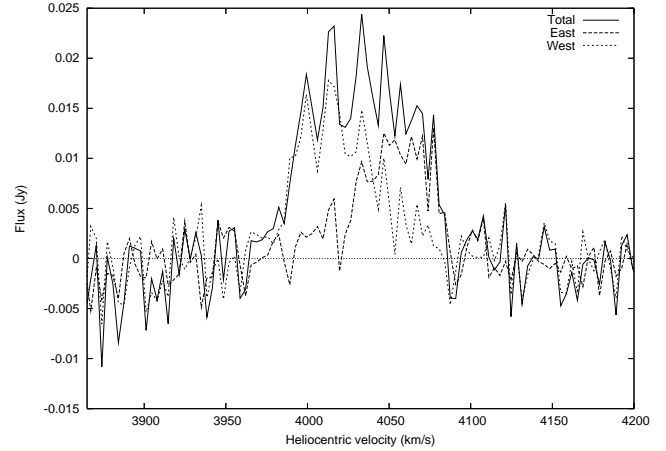


Figure 3. The spectra of SBS 0335–052E and SBS 0335–052W (left) are overlaid upon the spectrum of the whole system. These are obtained from data at an angular resolution of $\sim 43 \times 39$ arcsec².

Table 2. Main parameters of the observed galaxies.

Parameter	SBS 0335–052E	SBS 0335–052W
V_{hel} (km s ⁻¹)	4014.7	4053.6
$12 + \log(\text{O}/\text{H})$	7.29	7.12
H I flux (Jy km s ⁻¹)	0.61	0.86
M_{HI} ($10^8 M_{\odot}$)	4.2	5.8
$M_{\text{star}}/(M_{\text{star}} + M_{\text{gas}})$	0.07	0.016
M_{dyn} ($10^9 M_{\odot}$)	7.0	7.9

50.8 ± 3.3 and 47.4 ± 3.3 km s⁻¹. For the entire system, the central velocity is 4031.5 ± 1.7 km s⁻¹, the velocity range over which emission is detected is 73 km s⁻¹, while the total linear extent is ~ 58.5 kpc. Assuming the system is bound, its indicative dynamical mass can be estimated as:

$$M_{\text{ind}} = 2.3 \times 10^5 \times R_{\text{kpc}} \times V_{\text{km s}^{-1}}^2 M_{\odot} = \sim 9.0 \times 10^9 M_{\odot}.$$

The same formula gives indicative dynamical masses of $6.0 \times 10^9 M_{\odot}$ and $7.2 \times 10^9 M_{\odot}$ for the east (E) and west (W) galaxy, respectively (where we have assumed sizes of 10 and 13.6 kpc, and velocity widths of 51 and 48 km s⁻¹, respectively). The sum of the indicative dynamical masses of the two galaxies exceeds the total indicative dynamical mass, because the various inclination angles involved have not been correctly accounted for.

The indicative dynamical mass is ~ 10 times larger than the total gas mass. Using the stellar masses from Pustilnik et al. (2004), the $M_{\text{star}}/(M_{\text{star}} + M_{\text{gas}})$ ratio is 0.07 and 0.016 for the E and W galaxy, respectively. The various measured parameters for the two galaxies are summarized in Table 2.

4 STAR FORMATION IN SBS 0335–052

Current star formation in SBS 0335–052E is largely confined to several superstar clusters (SSCs), located in the central region of the galaxy (Thuan et al. 1997). The ages of the SSCs show a systematic variation with position, with the oldest SSCs being to the north and the youngest clusters being at the south-eastern tip (Thuan et al. 1997; Reines, Johnson & Hunt 2008;

Thompson et al. 2009). Reines et al. (2008) compute an age of ~ 15 Myr for the oldest SSCs and < 3 Myr for the youngest ones, and also determine that the star formation is propagating at a rate of $\sim 35 \text{ km s}^{-1}$. Thuan et al. (1997) also draw attention to a large ($\sim 380 \text{ pc}$) superbubble, which they identify as being a supernova blown cavity. Fig. 4(left) shows the H I emission (contours) at resolution of $\sim 7 \text{ arcsec}$ (1.8 kpc) overlaid on an *HST* Advanced Camera for Surveys (ACS) image. As can be seen, the H I contours in the north-west are aligned with the direction of the superbubble. The asymmetry of ionized gas, relative to the central starburst, is also seen on the data from Papaderos et al. (1998), Pustilnik et al. (2004), Izotov et al. (2006), and recent Fabry-Perot interferometry to study H α -kinematics (Pustilnik et al., in preparation). Note also that the north-west extensions of the H I contours are essentially due to material being pulled out to form the ‘bridge’ between SBS 0335–052E and W (see the lower resolution images, Fig. 1). At a still higher resolution of $\sim 4 \text{ arcsec}$ (1 kpc , Fig. 4(right)), one can see that the detected H I emission is confined to a region to the south-east of the southern most SSC. The sensitivity of the H I observations decreases with increasing spatial resolution, so the high resolution images detect only the highest column density gas. As can be seen from Fig. 4(left), the superbubble region corresponds to gas with column densities $\lesssim 9 \times 10^{20} \text{ atoms cm}^{-2}$, while the density in the south-east ridge (Fig. 4(right)) reaches up to $\sim 21 \times 10^{20} \text{ atoms cm}^{-2}$. The superbubble seems to have expanded preferentially into the lower density gas. The latter is produced when the ‘bridge’ material is being pulled out. The propagation of star formation towards the south-east could be due to the propagation of the superbubble into the relatively denser gas there.

In this context, it is interesting to note that the expansion velocity that Thuan et al. (1997) derive for the superbubble is $\sim 17 \text{ km s}^{-1}$, which is within a factor of ~ 2 of that derived for the propagation rate of the star formation. Given the large uncertainties in both these rates, agreement to within a factor of 2 is quite reasonable. The north-to-south propagation of the star formation, hence, appears to be attributable to the expansion of a superbubble into a medium in which there is an overall north-south density gradient because of the tidal interaction. Such a scenario would also provide a natural explanation for the dominant cluster mode of star formation observed in SBS 0335–052E. High pressures are expected in gas that is being compressed by an expanding supernova shell, and Elmegreen (2004) suggests that high pressure is conducive to the cluster mode of star formation. A similar pattern of sequential star formation and a dominant cluster mode for the star formation has recently been found associated with an expanding supernova shell in the outer galaxy (Kobayashi et al. 2008).

Given that SBS 0335–052E and W are among the lowest metallicity galaxies known, it is interesting to see if the star formation occurs at a similar gas threshold density as for more metal-rich galaxies. For example, Skillman (1987) suggested that star formation in dwarf galaxies occurs only when the gas column-density crosses a threshold value of $\sim 10^{21} \text{ atoms cm}^{-2}$; this in turn could be related to a threshold amount of dust shielding required for the production of molecular gas. In this case, one would expect that the threshold column-density increases with decreasing

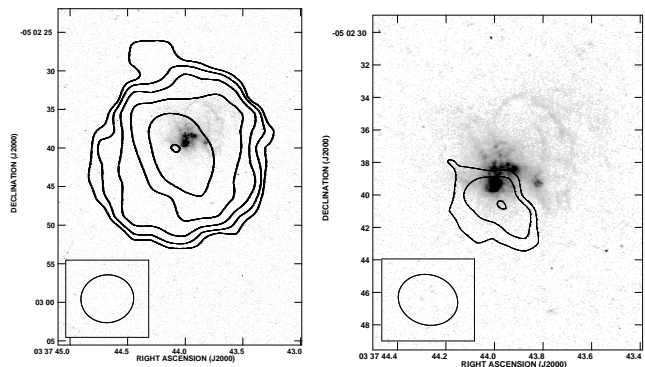


Figure 4. (Left.) The integrated H I intensity map of SBS 0335–052E, at an angular resolution of $\sim 7 \times 6 \text{ arcsec}^2$, in contours, overlaid on an *HST* ACS continuum image (grey-scale). The contours are at H I column densities of 1.3, 2.3, 4.0, 6.9, 11.9, $20.6 \times 10^{20} \text{ atoms cm}^{-2}$. The grey-scale is in arbitrary units. **(Right.)** Same as on the left, except that the resolution of the H I image is $\sim 4 \times 3 \text{ arcsec}^2$, and the contours are at H I column densities of 8.7, 13.2, $20.1 \times 10^{20} \text{ atoms cm}^{-2}$.

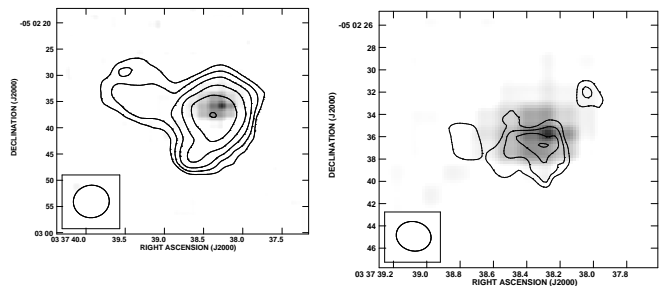


Figure 5. (Left.) The integrated H I intensity map of SBS 0335–052W, at an angular resolution of $\sim 7 \times 6 \text{ arcsec}^2$, in contours, overlaid on an DSS-II *B*-band image (grey-scale). The contours are at H I column densities of 3.6, 5.3, 7.7, 11.4, 16.7 and $24.6 \times 10^{20} \text{ atoms cm}^{-2}$. The grey-scale is in arbitrary units. **(Right.)** Same as on the left, except that the resolution of the H I image is $\sim 2.9 \text{ arcsec}$, and the contours are at H I column densities of 1.6, 2.3, 3.3 and $4.7 \times 10^{21} \text{ atoms cm}^{-2}$.

gas-phase metallicity. Schaye (2004) (see also Schaye 2008; Schaye & Dalla Vecchia 2008) suggests a different model, one in which star formation is related to the formation of a cold phase of the interstellar medium. From his fitting formulae for the threshold column density, the threshold density increases with increasing gas fraction and decreasing metallicity (all other factors being equal). In this model too, gas-rich XMD galaxies should have a higher threshold for star formation than spirals. This issue was also explored, in detail, in Ekta et al. (2008), who found no conclusive evidence for an increase in threshold density with metallicity, albeit in a relatively small sample of XMD galaxies.

The H I column densities at the positions of the brightest star-forming regions in SBS 0335–052E and SBS 0335–052W are ~ 2.0 and $5.4 \times 10^{21} \text{ atoms cm}^{-2}$, respectively. The measurements were made at a resolution of ~ 3.4 and 2.75 arcsec (880 and 715 pc), respectively. The signal-to-

noise ratio for SBS 0335–052E was too low for the column density to be measured at the higher resolution used for SBS 0335–052W. In SBS 0335–052E, the H I peak is slightly (i.e., ~ 1.5 arcsec, or 0.4 kpc), offset from the brightest star-forming region (as was already noticed from the VLA data (Pustilnik et al. 2001)). Nevertheless, it lies within a half beam-width of the latter. The western H I peak is also slightly (~ 1 arcsec, or 0.26 kpc) offset from the brightest star-forming region in SBS 0335–052W. Note that the column densities have not been corrected for inclination, because, as discussed above, it is difficult to estimate the inclination angles of the H I discs. The H I column density of SBS 0335–052E, as calculated from its *HST* spectral observations by Thuan & Izotov (1997), is $7.0 \pm 0.5 \times 10^{21}$ atoms cm^{-2} . The higher value that they obtain is presumably a result of the much higher angular resolution of the *HST* data. These peak H I column densities, are amongst the largest values found in gas-rich dwarf or XMD galaxies (see, e.g., Taylor et al. 1994; van Zee et al. 1998; Begum et al. 2006; Ekta et al. 2006; Ekta et al. 2008). This is despite the fact that all the above mentioned studies have better linear resolution than that of our observations, except for a few galaxies in Taylor et al. (1994). Given the uncertain inclination correction however, it is difficult to gauge the significance of this higher observed H I column density.

5 DISCUSSION AND SUMMARY

SBS 0335–052 is the lowest metallicity star-forming system known. The system is further peculiar in being an interacting pair of dwarf galaxies. In the case of SBS 0335–052E, the metallicity is low not just in the ionized H II regions, but also in the surrounding H I gas. From FUSE observations, Thuan, Lecavelier des Etangs & Izotov (2005) find that the metallicity in the H I envelope is similar to that in the central star-forming regions.

Our H I data shows that the pair is in an advanced stage of interaction, with the gas being pulled out to form a bridge, as well as into elongated tidal tails. As discussed in Section 3, if the dynamic-to-baryonic mass ratio is $\gtrsim 10$, the system is bound, and will eventually merge. The relatively short tails, and the faintness of the ‘bridge’ then suggest that the pair is probably past its first close encounter, but has yet to fall towards each other for the second time (see, e.g., Toomre & Toomre 1972). di Matteo et al. (2008) show that starbursts can be triggered in extremely gas-rich galaxies, which are undergoing their first close encounter, depending on the details of the galaxy structure and the orbit geometry. The starburst onset could range from being just before the first close encounter (e.g., for very close, planar encounters) to 0.1–0.4 Gyr after the encounter. The relatively broad tidal features (as opposed to the narrow long features produced by direct encounters) also suggest that neither of the galaxies is undergoing a direct encounter (see, e.g., Howard et al. 1993). Indeed from Fig. 1, one can see that if the elongated structure seen in the central regions of SBS 0335–052W reflects the underlying gas disc, the galaxy is undergoing a highly inclined encounter.

Interestingly, all of the six lowest-metallicity star-forming XMD galaxies known are either currently undergoing tidal interactions, or appear to be the remnants of a

merger of extremely gas-rich progenitors (Ekta et al. 2008). While interactions have long been regarded as triggers for starbursts, numerical simulations show that, in fact, only a small fraction of all binary interactions lead to a reasonably strong starburst (di Matteo et al. 2008). The enhancement in the star formation rate during merger depends on a number of factors, but in general (in recent models) the internal structure (e.g., presence of a bulge, gas-mass fraction, disc-stability factor, etc.) appear to play a more crucial role in determining the strength and duration of the starburst than the interaction geometry (Mihos & Hernquist 1996; di Matteo et al. 2008). In particular, for gas-rich galaxies, di Matteo et al. (2008) find that the amplitude of the starburst, which occurs just after the first close passage, is generally stronger than for gas-poor galaxies.

In the current situation, the galaxies concerned are both extremely gas-rich dwarfs, and are likely to have similar internal structure. While numerical simulations of such systems are very limited, for somewhat less gas-rich systems, Mihos & Hernquist (1996) show that coplanar orbits lead to somewhat stronger starbursts than inclined orbits. As discussed above, SBS 0335–052W appears to be undergoing an inclined encounter, which could perhaps be the reason for its relatively lower star formation rate. As far as simulations of interacting, gas-rich galaxies are concerned, Springel & Hernquist (2005) show that a direct encounter between two giant, extremely gas-rich discs can lead to the formation of spiral-galaxy-like gas-rich remnant. The star formation rate is enhanced both during the first close passage as well as during the final merger. In general, gas-rich mergers tend to show larger enhancements in the instantaneous star formation rate than gas-poor ones, both because there is more raw material available for star formation, and also because of the inherent instability of thin gas discs (di Matteo et al. 2008).

We used the recently released Identikit tool (Barnes & Hibbard 2009) to model the interaction in the SBS 0335–052 system. Since Identikit is based on collisionless N-body simulations, we compare only the morphology of the outer regions and the velocity-field projections. The best possible match, that we could find, is shown in Fig. 6, along with the data projections in the same co-ordinate system. While the match is not perfect (given the limitations of the model, a perfect match is perhaps not to be expected) the parameters from the match could be taken as indicative. In the displayed model, the galaxies undergo a close (pericenter distance of ~ 0.55 kpc) encounter, which is somewhat retrograde encounter for SBS0335–052E, and close to polar for SBS 0335–052W. The sky plane is inclined ~ 45 degrees with respect to the orbit plane. The observed snapshot corresponds to shortly (~ 0.1 Gyr) after the first perigalacticon. From optical colours, the major enhanced star formation in both components is estimated to have started 0.1–0.4 Gyr ago. It is interesting to note that this is consistent with the star formation activity starting just before the pericenter passage, as predicted for some cases of very close encounters in gas-rich mergers (di Matteo et al. 2008). A more detailed simulation of this unique pair would be highly desirable.

While the interaction in SBS 0335–052 is likely to have triggered the current starburst, it almost certainly plays an important role in the long-term evolution of the sys-

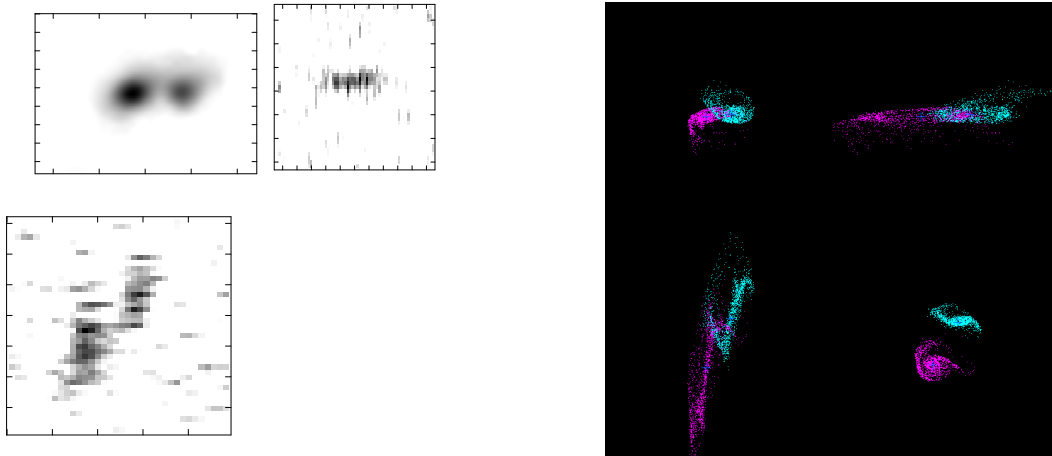


Figure 6. **Left:** Projections of the HI data cube, made for comparison with the Identikit model. The panels (clockwise and starting from the upper left) are **(1)** The sky (X, Y) plane projection of the HI in SBS 0335–052 system, at an angular resolution of ~ 40 arcsec. Note that the RA (‘ X ’) axis is flipped with respect to Fig. 1, so the E galaxy is to the right. **(2)** The V, Y plane projection (where ‘ V ’ is the velocity). **(3)** The X, V plane projection. **Right:** Identikit web interface results for the closest fit model that we could make for our data. The panels are in the same order as for the observed HI data. The lower right panel is the X, Z plane projection, where Z is the depth along the line of sight (for which there is no counterpart in the left panel, since the Z co-ordinate is not an observable). Blue dots correspond to the first galaxy, and pink ones correspond to the second galaxy. The input parameters used in the model are pericenter distance $p = 0.125$ ($1.5 h$), inclinations of galaxy spins relative to the orbital plane $i_1=130, i_2=70$ degrees, azimuthal orientations $\omega_1=340, \omega_2=90$ degrees, the angles between the sky plane and the orbital plane, $\theta_X=45$ and $\theta_Y=45$ degrees. The rotation angle around Z -axis is 310 degrees. The snapshot is for a time $t \sim 0.5$ (or ~ 70 Myr, in physical units), after the first close passage. The conversion from dimensionless units to physical units was done assuming that the galaxies in SBS 0335–052 system have scale-length, $h \sim 0.37$ kpc and, $V_{\text{rot}} \sim 40 \text{ km s}^{-1}$.

tem. Bekki (2008) presents results from numerical simulations of gas-rich dwarf galaxies, and shows that in the case where there is no stellar bulge, and the gas is initially in a cold disc, the merger remnant resembles a moderately gas-rich BCD (blue compact dwarf) galaxy. The central compact emission comes from a starburst triggered by the inflow of gas from the outskirts of the initial cold disc. High gas pressures in the star-forming regions also lead to the formation of massive star clusters (as seen for SBS 0335–052E). As mentioned above, the role of high pressures in forming massive star clusters was also discussed earlier by Elmegreen, Kaufman & Thomasson (1993) and Elmegreen (2004). Further, di Matteo et al. (2008) find that the strength of the central starburst found in merging gas-rich galaxies depends critically on the assumed disc stability. Simulations in which gas dissipation has been decreased to prevent excessive disc fragmentation for isolated galaxies (e.g., their particle-mesh - sticky-particles (PM-SM) simulation) show very little enhancement of star formation during the merger. Further, even in their simulations which do show an enhancement in the star formation rate, the major cause of the enhancement is induced disc instabilities, and not inflow of gas. While a significant radial metallicity gradient is known to exist in large spiral galaxies, such strong gradients have not been found in dwarf galaxies, and hence, the role that infalling gas plays in lowering the metallicity of the central regions may not be important.

Inflow of metal-poor gas is one possible cause for sizeable metal deficiency in central star-forming regions of some dwarf galaxies. Other possible causes are (a) preferential loss of metal-enriched gas, i.e., escape of supernova metal-enriched material from previous starbursts, (b) infall of pris-

tine ‘gas clouds’ from the intergalactic medium, (c) very slow evolution of locally very stable gas discs (extreme low surface brightness (LSB) galaxies), which fortuitously (e.g., due to residing in a void) escaped strong external disturbances and related additional star formation, and (d) a genuinely young galaxy which has not undergone much star formation (i.e., due to a too small an age).

Numerical simulations (e.g., Fragile et al. 2004) show that sufficiently strong starbursts, in sufficiently small galaxies, could indeed lead to significant outflow of metal-enriched gas. A high spatial and velocity resolution study of the ionized gas around the starburst region in SBS 0335–052E has indeed identified a high velocity ($\sim 50 \text{ km s}^{-1}$) outflow (Izotov et al. 2006). The final fate of this outflowing gas (i.e., whether it escapes from the galaxy or falls back to form a ‘galactic fountain’) depends on several parameters, including the mass of the parent galaxy, the presence of a hot-gas halo from the previous star formation activity, etc.. In addition, the positive feedback from massive, compact superstar clusters could also inhibit outflow of gas (e.g., Tenorio-Tagle et al. 2005, 2007; Wünsch et al. 2008). As far as infall of pristine gas clouds is concerned, our present data does not show any evidence for this, although the possibility that higher sensitivity data may show such clouds cannot be ruled out.

The SBS 0335–052 system is especially unusual in that both galaxies in the pair are extremely metal-deficient, with metallicities differing by only a factor ~ 1.5 . One possible explanation for their similar metallicities is that there has been an exchange and mixing of gas during their interaction. However, this seems unlikely, because of the faintness of the observed ‘bridge’, and also because gas exchange is

not believed to be very efficient during the first encounter of equal-mass galaxies (Toomre & Toomre 1972). It seems likely therefore, that the similar metallicities of these two galaxies are due to similar evolutionary histories. In this context, it is interesting to note that the SBS 0335–052 system is located near the edge of a large void (Peebles 2001), and that there appears to be, in general, an indication of excess of metal-deficient galaxies in voids (Pustilnik et al. 2006; Pustilnik & Kniazev 2007).

It is also interesting to note that the most metal-poor galaxies known, viz., SBS 0335–052, I Zw 18 and DDO 68, all appear to be interacting or merger remnants. Indeed, in the order given above, one could take these galaxies as forming a ‘merger sequence’, (with SBS 0335–052 being just past the first close passage, DDO 68 being a merger remnant (Ekta et al. 2008; Pustilnik, Tepliakova & Kniazev 2008) and I Zw 18 (van Zee et al. 1998) being at an intermediate phase) of extremely gas-rich galaxies.

To summarize, our multi-resolution H I observations show that the SBS 0335–052 system consists of a merging galaxy pair. At the lowest resolution, we see a faint diffuse ‘bridge’ joining the two galaxies (although the possibility of all of the observed emission arising from beam smearing can not be completely ruled out), while at higher resolutions, we see both H I concentrations around the stellar bodies as well as elongated tidal tails. The velocity fields are complex, and, at large-scales are dominated by the velocity difference between the galaxies and the velocity gradient along the tidal tails. At still higher resolution, we see that in SBS 0335–052E, the ionized superbubble identified in the *HST* images by Thuan et al. (1997) is extended along one of the tidal tails, while there is a clump of high-density H I gas at the other end of the superbubble. This is consistent with a scenario, in which the propagating star formation seen in this galaxy is driven by a superbubble expanding into a medium with a tidally-produced density gradient. In contrast to SBS 0335–052E, the higher resolution maps for SBS 0335–052W suggest that it is undergoing a somewhat polar encounter. Given the similar H I parameters of both galaxies, this difference in encounter geometry is possibly the reason for the weaker tidal disturbance and the resulting large difference in the past and current star formation in the E and W components.

ACKNOWLEDGEMENTS

We thank the staff of the GMRT who have made these observations possible. The GMRT is run by the National Centre for Radio Astrophysics of the Tata Institute of Fundamental Research. Partial support for this work was provided by ILTP grant B-3.13. SAP appreciates the partial support of this work through the Russian Foundation for Basic Research (RFBR) grant 06–02–16617 and the Russian Federal Agency on Education, project code 2.1.1/1937. The authors appreciate the assistance of the ‘Identikit’ authors J. Barnes and J. Hibbard.

REFERENCES

- Asplund M., Grevesse N., Sauval A.J., Allende Prieto C., Kiselman D., 2004, *A&A*, 417, 751
- Barnes J.E., Hibbard J.E., 2009, *AJ*, 137, 3071
- Begum A., Chengalur J.N., Karachentsev I.D., Kaisin S.S., Sharina M.E., 2006, *MNRAS*, 365, 1220
- Bekki K., 2008, *MNRAS*, 388, L10
- Chengalur J.N., Pustilnik S.A., Martin J.-M., Kniazev A.Y., 2006, *MNRAS*, 371, 1849
- di Matteo P., Bournaud F., Martig M., Combes F., Melchior A.-L., Semelin B., 2008, *A&A*, 492, 31
- Ekta, Chengalur J.N., Pustilnik S.A., 2006, *MNRAS*, 372, 853
- Ekta, Chengalur J.N., Pustilnik S.A., 2008, *MNRAS*, 391, 881
- Elmegreen B.C., 2004, in Lamers H.J.G.L.M., Smith L.J., Nota A., eds, *ASP Conf. Ser. Vol. 322, The Formation and Evolution of Massive Young Star Clusters*. Astron. Soc. Pac., San Francisco, p. 277
- Elmegreen B.G., Kaufman M., Thomasson M., 1993, *ApJ*, 412, 90
- Fragile P.C., Murray S.D., Lin, D.N.C., 2004, *ApJ*, 617, 1077
- Howard S., Keel W. C., Byrd G., Burkey J., 1993, *ApJ*, 417, 502
- Izotov Y.I., Lipovetsky V.A., Chaffee F.H., Foltz C.B., Guseva N.G., Kniazev A.Y., 1997, *ApJ*, 476, 698
- Izotov Y.I., Thuan T.X., Guseva N.G., 2005, *ApJ*, 632, 210
- Izotov Y.I., Schaerer D., Blecha A., Royer F., Guseva N.G., North P., 2006, *A&A*, 459, 71
- Kobayashi N., Yasui C., Tokunaga A. T., Saito M., 2008, *ApJ*, 683, 178
- Kunth D., Östlin G., 2000, *A&AR*, 10, 1
- Mihos J.C., & Hernquist L., 1996, *ApJ*, 464, 641
- Papaderos P., Izotov Y.I., Fricke K.J., Thuan T.X., Guseva N.G., 1998, *A&A*, 338, 43
- Peebles P.J.E., 2001, *ApJ*, 557, 495
- Pustilnik S.A., Kniazev A.Y., 2007, in Combes F., Palous J., eds, *Proc. IAU Symp. 235, Galaxy evolution across the Hubble time*, Prague, p. 238
- Pustilnik S.A., Martin J.-M., 2007, *A&A*, 464, 859
- Pustilnik S.A., Brinks E., Thuan T.X., Lipovetsky V.A., Izotov Y.I., 2001, *AJ*, 121, 1413
- Pustilnik S.A., Kniazev A.Y., Pramskij A.G., Ugryumov A.V., 2003, *Ap&SS*, 284, 795 (astro-ph/0301089)
- Pustilnik S.A., Pramskij A.G., Kniazev A.Y., 2004, *A&A*, 425, 51
- Pustilnik S.A., Engels D., Kniazev A.Y., Pramskij A.G., Ugryumov A.V., Hagen H.-J., 2006, *Astronomy Letters*, 32, 228
- Pustilnik S.A., Tepliakova A.L., Kniazev A.Y., 2008, *Astronomy Letters*, 34, 457
- Reines A.E., Johnson K.E., Hunt L.K., 2008, *AJ*, 136, 1415
- Schaye J., 2004, *ApJ*, 609, 667
- Schaye J., 2008, in Davies J.I., Disney M.J., eds, *Proc. IAU Symp. 244, Dark galaxies and lost baryons*, p. 247 (astro-ph/0708.3366)
- Schaye J., Dalla V.C., 2008, *MNRAS*, 383, 1210
- Skillman E.D., 1987, in Persson C.J.L., eds, *NASA Conf. Publ. Vol. 2466, Star formation in galaxies*, Pasadena, p. 263

- Springel V., Hernquist L., 2005, *ApJ*, 622, L9
- Taylor C.L., Brinks E., Pogge R.W., Skillman E.D., 1994, *AJ*, 107, 971
- Tenorio-Tagle G., Silich S., Rodriguez-Gonzalez A., Munoz-Tunon C., 2005, *ApJ*, 628, L13
- Tenorio-Tagle G., Wünsch R., Silich S., Palous J., 2007, *ApJ*, 658, 1196
- Thompson R.I., Sauvage M., Kennicutt R.C., Engelbracht C., Vanzi L., Schneider G., 2009, *ApJ*, 691, 1068
- Thuan T.X., Izotov Y.I., 1997, *ApJ*, 489, 623
- Thuan T.X., Izotov Y.I., Lipovetsky V.A., 1997, *ApJ*, 477, 661
- Thuan T.X., Lipovetsky V.A., Martin J.-M., Pustilnik S.A., 1999, *A&AS*, 139, 1
- Thuan T.X., Lecavelier des Etangs A., Izotov Y.I., 2005, *ApJ*, 621, 269
- Toomre A., Toomre J., 1972, *ApJ*, 178, 623
- van Zee L., Westpfahl D., Haynes M.P., Salzer J.J., 1998, *AJ*, 115, 1000
- Wünsch R., Tenorio-Tagle G., Palous J., Silich S., 2008, *ApJ*, 683, 683